Are your MRI contrast agents cost-effective?
Learn more about generic Gadolinium-Based Contrast Agents.
FRESENIUS KABI
caring for life

AJNR

MR of the normal neonatal brain: assessment of deep structures.

A J Barkovich

AJNR Am J Neuroradiol 1998, 19 (8) 1397-1403
http://www.ajnr.org/content/19/8/1397

This information is current as of April 18, 2024.

AJNR Am J Neuroradiol 19:1397–1403, September 1998

MR of the Normal Neonatal Brain: Assessment of Deep Structures

A. James Barkovich

BACKGROUND AND PURPOSE: **MR imaging is a powerful tool for studying the anatomy of and the developmental changes that occur in the brain. The purpose of this project was to determine which structures can be distinguished on standard spin-echo MR sequences of a normal neonatal brain and with what frequency they can be identified.**

METHODS: **The T1- and T2-weighted spin-echo MR images of 12 term neonates, all of whom had normal neonatal courses and were neurologically and developmentally normal at age 12 months, were reviewed retrospectively. All structures that differed in signal intensity from unmyelinated gray matter and unmyelinated white matter were recorded.**

RESULTS: **In general, myelinated gray matter structures, such as cranial nerve nuclei and other nuclei of the brain stem and deep cerebrum, were the structures best seen on T2-weighted images. Most of these nuclei were seen in 75% to 100% of our subjects on T2-weighted images. They were seen less well on T1-weighted images. Myelinated white matter structures, particularly axonal tracts, were the structures best seen on T1-weighted images. The medial and lateral lemnisci, median longitudinal fasciculus, optic tracts, superior and inferior cerebellar peduncles, and the posterior limbs of the internal capsules were seen in 75% to 100% of our subjects on T1-weighted images. Except for the posterior limbs of the internal capsules, these structures were seen less well on T2-weighted images.**

CONCLUSION: **A large number of small structures, such as the nuclei of the brain stem and deep cerebral nuclei, can be routinely identified on standard spin-echo MR imaging sequences. A knowledge of these structures is essential to proper interpretation of imaging studies in neonates and infants.**

During the past 10 years, MR imaging has been an extremely useful tool in the assessment of the neonatal brain (1–16). Since the time of the initial studies, significant advances have been achieved in the quality of MR images obtained on standard commercially available MR scanners, yet no attempts have been made to reassess the ability of MR imaging to detect small structures within the neonatal brain and, particularly, within the brain stem. Since cranial neuropathies are a common indication for MR imaging in neonates, a knowledge of the normal MR appearance of the neonatal brain stem is crucial.

As a result of an ongoing study of neonates with intrapartum difficulties, we have had the opportunity to perform high-quality MR examinations of the brain on 12 infants who had normal postdelivery neonatal courses and normal neurologic and developmental examinations at age 12 months. The analysis of these MR studies form the basis for this report.

Received January 20, 1998; accepted after revision April 2.

Supported in part by NIH grant P50 NS35902 and by NIH grant M01RR01271, the Pediatric Clinical Research Center.

From the Department of Radiology/Section of Neuroradiology, Box 0628, L371, University of California, San Francisco, 505 Parnassus Ave, San Francisco, CA 94143. Address reprint requests to A. James Barkovich, MD.

© American Society of Neuroradiology

Methods

During the course of a prospective study analyzing the imaging findings in neonates who suffered distress during birth, 12 patients were identified who had normal findings on MR studies, normal neonatal courses, normal results of neurologic examinations at 3 and 12 months, and normal cognition and development (as determined by the Bayley Scores of Infant Development II [17]) at age 12 months. These patients composed the cohort for this study.

The 12 patients were born after gestation periods of 38 to 40 weeks (mean, 39 weeks). The MR studies were performed at ages ranging from 1 day to 7 days after birth (mean age, 4 days; median age, 4 days). The MR imaging sequences reviewed for this study consisted of two sequences. A standard spin-echo T1-weighted sequence was acquired with imaging parameters of 500/11/2 (TR/TE/excitations). Section thickness was 4 mm (1-mm gap), with an 18-cm field of view, and a 256 × 192 imaging matrix. A standard spin-echo T2-weighted sequence used imaging parameters of 3000/120/1, with a 4-mm section thickness and a 2-mm gap. All other parameters were the same as for the T1-weighted sequence.

The MR examinations were analyzed in an attempt to record all structures with signal intensity differing from unmy-

TABLE 1: Frequency of identification of gray matter structures with signal different than unmyelinated cortex

Structure	Frequency of Identification on T1	Frequency of Identification on T2
Nucleus CN III	0/12	7/12
Nucleus CN V	0/12	8/12
Nucleus CN VI	0/12	8/12
Nucleus CN VII	1/12	9/12
Nucleus CN VIII	0/12	6/12
Nucleus CN XII	0/12	2/12
Inferior olivary nucleus	0/12	3/12
Gracile nucleus	0/12	9/12
Cuneate nucleus	0/12	7/12
Interpeduncular nucleus	0/12	7/12
Nucleus inferior colliculus	0/12	11/12
Cerebellar dentate nucleus	0/12	11/12
Globus pallidus	12/12	0/12
Far lateral putamen	0/12	11/12
Caudate	0/12	0/12
Claustrum	0/12	11/12
Subthalamic nucleus	4/12	9/12
Lateral geniculate nucleus	3/12	10/12
Medial geniculate nucleus	2/12	12/12
Ventrolateral thalamus	12/12	12/12
Flocculus cerebelli	9/12	10/12
Cerebellar vermis	9/12	10/12

Note.—T1 indicates T1-weighted sequence; T2, T2-weighted sequence; CN, cranial nerve.

TABLE 2: Frequency of identification of white matter structures with signal intensity different than unmyelinated white matter

Structure	Frequency of Identification on T1	Frequency of Identification on T2
Medial lemniscus	12/12	3/12
Decussation of medial lemniscus	3/12	0/12
Lateral lemniscus	9/12	3/12
Median longitudinal fasciculus	9/12	3/12
CN V (in pons)	3/12	0/12
Dorsal medullary fasciculi	3/12	0/12
Brachium of inferior colliculus	5/12	0/12
Spinal tract of CN V	3/12	0/12
Inferior cerebellar peduncle	10/12	6/12
Superior cerebellar peduncle	10/12	6/12
Decussation of superior cerebellar peduncles	9/12	1/12
Posterior limb internal capsule	12/12	12/12
Anterior limb internal capsule	0/12	0/12
Optic nerve	0/12	0/12
Optic chiasm	0/12	1/12
Optic tracts	7/12	0/12
Optic radiations	1/12	2/12
Corpus callosum	0/12	0/12
Anterior commissure	3/12	0/12
Habenular commissure	1/12	0/12
Corticospinal tracts	11/12	9/12

Note.—T1 indicates T1-weighted sequence; T2, T2-weighted sequence; CN, cranial nerve.

elinated white matter or gray matter in the brain on both the T1- and T2-weighted images. Thus, all white matter foci that were hyperintense relative to unmyelinated white matter on T1-weighted images and hypointense relative to unmyelinated white matter on the T2-weighted images were distinguished. Similarly, gray matter foci that were of higher signal than unmyelinated cortex on T1-weighted images and of lower signal than unmyelinated cortex on T2-weighted images were also recorded. These structures were then identified by consulting a neuroanatomy textbook and recorded on a chart. After the imaging studies of all 12 patients were analyzed, the frequency with which each structure was identified was assessed.

Results

The structures identified on T1-weighted images were mostly white matter tracts, and the structures identified on T2-weighted images were primarily gray matter structures (nuclei). The structures and the frequency with which they were detected are listed in Tables 1 and 2.

Medulla

On T1-weighted images, the most commonly identified structures were the median longitudinal fasciculus, the inferior cerebellar peduncles, and the medial lemniscus (Fig 1A). The decussation of the medial lemnisci, the spinal tract of the fifth cranial nerve, and the cuneate and gracile fasciculi were each identified in 25% of patients.

On T2-weighted images, the gracile and cuneate nuclei were identified in most patients (Fig 2A). The vestibular nuclei (Fig 2B and C) and inferior cerebellar peduncles (Fig 2B) were identified in about half the patients. The hypoglossal nuclei, the inferior olivary nuclei, the medial lemnisci, and the median longitudinal fasciculi were identified in 25% of patients or fewer.

Pons

On T1-weighted images through the pons, the medial lemnisci and superior cerebellar peduncles were essentially always seen (Fig 1B). The lateral lemnisci and the median longitudinal fasciculi were usually seen. The fascicles of the fifth cranial nerves were sometimes seen coursing through the pons (Fig 1B).

On T2-weighted images, the nuclei of the fifth, sixth, and seventh cranial nerves were identified in most subjects (Fig 2D). The superior cerebellar peduncles, the medial and lateral lemnisci, and the medial longitudinal fasciculi were seen as discrete structures in 25% to 50% of subjects (Fig 2E); it was more common to see a nondiscrete blur of low intensity, consisting of the medial and lateral lemnisci, the axons of the superior cerebellar peduncles, and the median longitudinal fasciculus in the dorsal upper pons.

Midbrain

On T1-weighted images through the midbrain, high signal from the decussation of the superior cerebellar peduncles, with possibly some contribution from the third nerve nuclei, was commonly identified (Fig 1C),

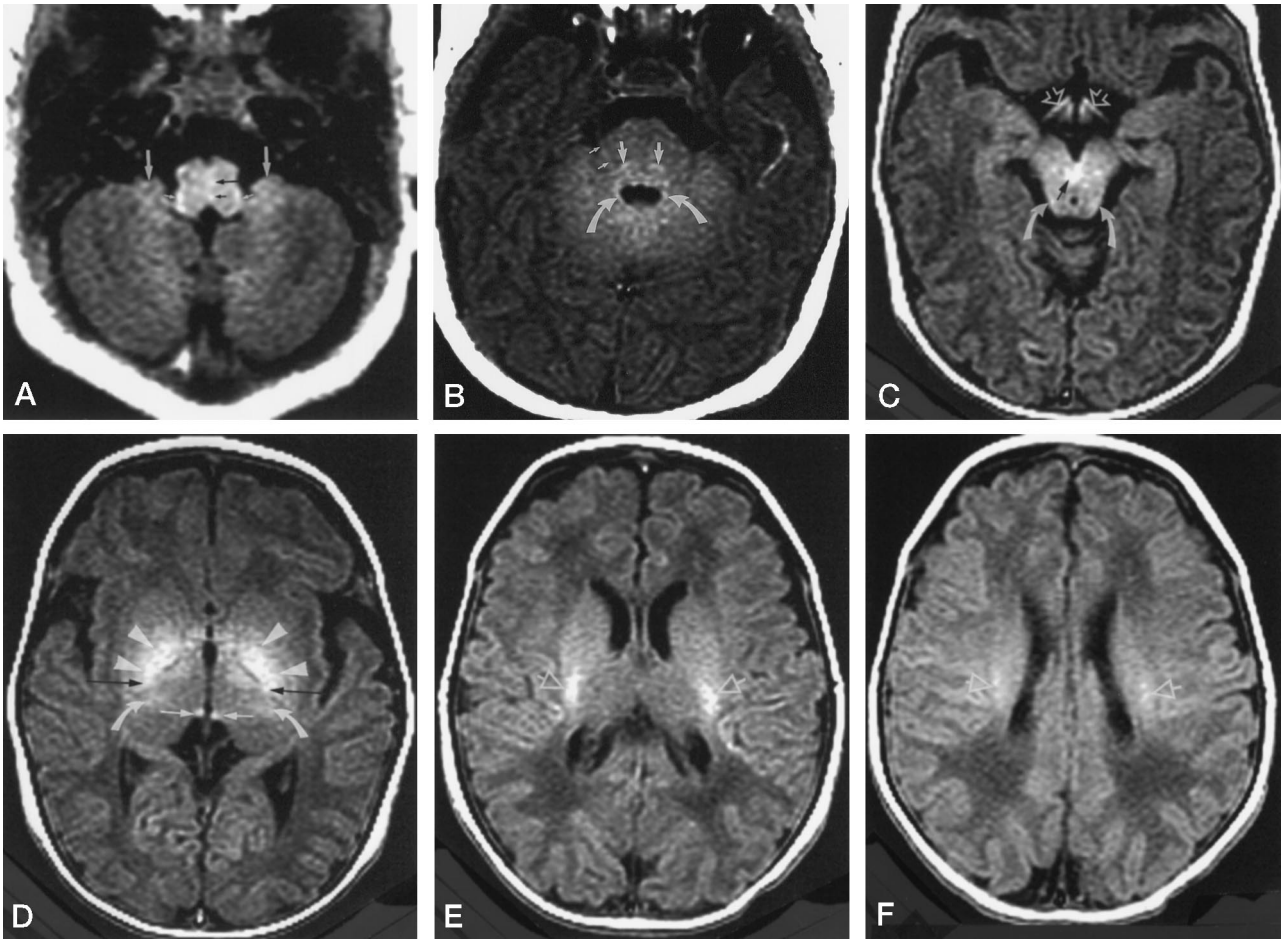

FIG 1. Axial spin-echo (500/11/2) images.

A, Image at the level of the medulla shows hyperintensity of the flocculi (*large white arrows*), inferior cerebellar peduncles (*small white arrows*), medial lemniscus (*large black arrow*), and median longitudinal fasciculus (*small black arrow*).

B, Image at the level of the midpons shows the curvilinear hyperintensity of the medial lemniscus (*large straight arrows*) and the high intensity of the superior cerebellar peduncles (*curved arrows*) at the lateral aspects of the fourth ventricle. The fascicle of the right fifth cranial nerve is seen coursing through the pons (*small arrows*).

C, Image at the level of the midbrain shows high signal at the decussation of the superior cerebellar peduncles (*black arrow*) with possibly some contribution from the nuclei of the third cranial nerves. A curvilinear stripe of hyperintensity is seen in the dorsolateral margins of the midbrain (*curved arrows*), representing the brachium of the inferior colliculus. Some hyperintensity is seen in the optic tracts (*open arrows*). Note that at this level, the cerebral white matter is of uniform low intensity and the cerebral cortex is of uniform intensity other than some slight hyperintensity in the visual cortex.

D, Image at the level of the basal ganglia shows high signal intensity in the globi pallidi (*arrowheads*), the posterior limbs of the internal capsules (*black arrows*), the ventrolateral thalamic nuclei (rather faint) (*curved arrows*), and the habenular commissure (*straight white arrows*).

E and *F*, Images at higher levels show hyperintensity (*arrows*) along the corticospinal tracts.

as were the more rostral extensions of the medial and lateral lemnisci. The brachium of the inferior colliculus was identified in about half the subjects (Fig 1C).

On T2-weighted images, the nucleus of the inferior colliculus (Fig 2F) was almost always identified. The nuclei of the third cranial nerves and the interpeduncular nuclei were identified in more than half our subjects (Fig 2F). The superior cerebellar peduncles had low signal intensity in half our subjects.

Cerebellum

On T1-weighted images, the cerebellar vermes (Fig 1A) and flocculi (Fig 1A) had high signal intensity in nine patients. On T2-weighted images, the cerebellar dentate nuclei were always distinguished by an irregular circumference of hypointensity around a hyperintense center (Fig 2C). The cerebellar vermes and flocculi were of low signal intensity in 10 of 12 subjects (Fig 2B–D).

Deep Cerebral Nuclei and Optic Pathways

On T1-weighted images through the deep cerebral nuclei and internal capsules, a focus of high-signal intensity was always seen in the posterior limb of the internal capsules (Fig 1D). The globi pallidi, particularly in the medial aspects, were always of slightly higher signal intensity than the other gray matter nuclei, as were the ventrolateral thalamic nuclei (Fig 1D). The high signal previously attributed to the posterior half of the posterior limbs of the internal cap-

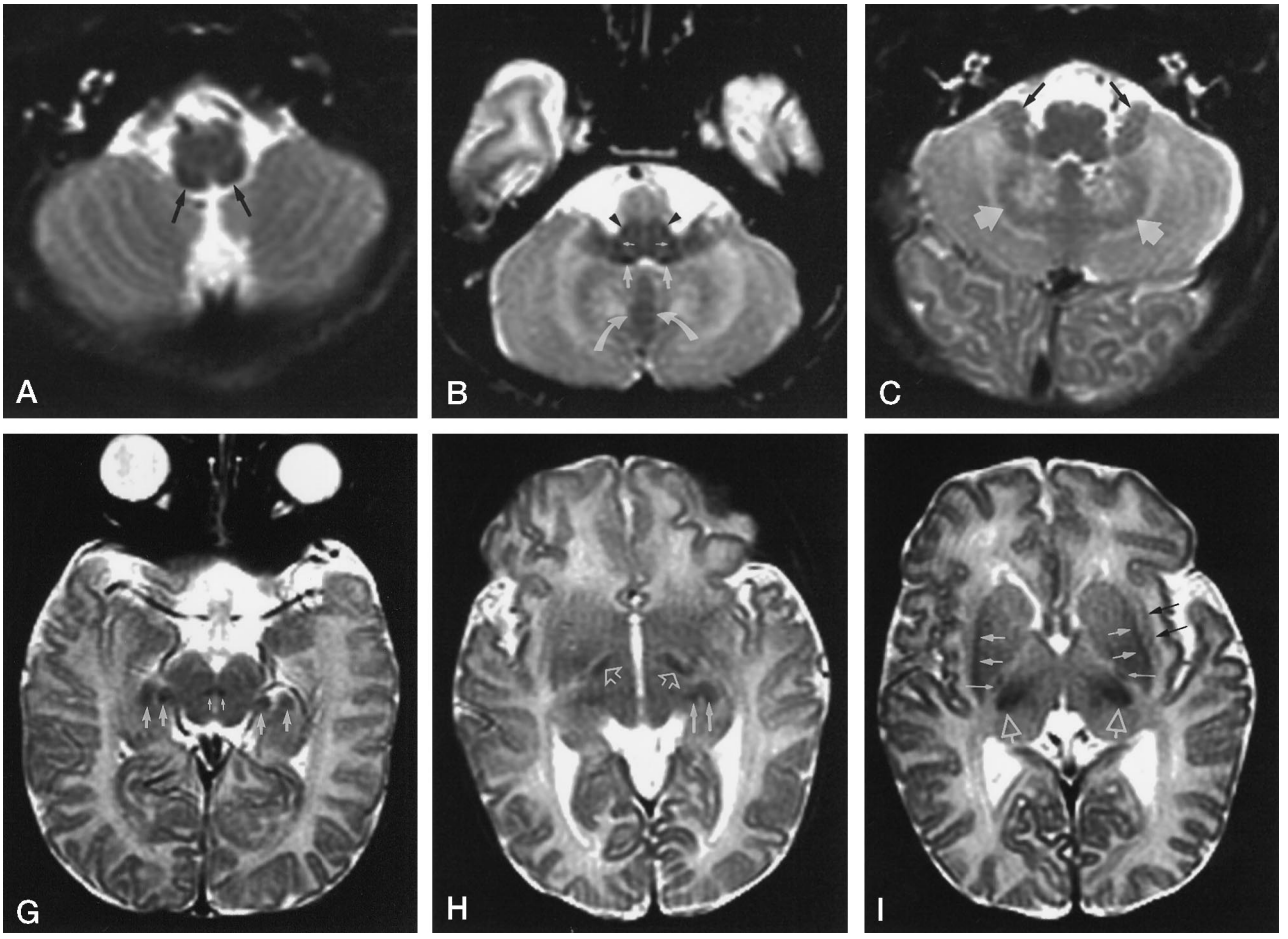

sules (1) appeared to be primarily in the medial aspect of the globi pallidi on these high-quality images (Fig 1D). The optic tracts were of high signal intensity in about half our subjects (Fig 1C). The optic nerves and optic chiasm were very difficult to evaluate because of the contrast from the surrounding fat and CSF. The medial and lateral geniculate bodies, subthalamic nuclei, and optic radiations were less commonly identified as regions of high signal intensity.

On T2-weighted images, a spot of low signal intensity was always seen in the posterior aspect of the posterior limb of the internal capsule (Fig 2I). In addition, discrete low signal intensity was always seen in the medial geniculate bodies (Fig 2G) and the ventrolateral thalamic nuclei (Fig 2I). Low signal intensity was nearly always seen in a curvilinear area of the far lateral putamina (Fig 2I), in the claustra (Fig 2I), in the subthalamic nuclei (Fig 2H), and in the lateral geniculate bodies (Fig 2G and H). The optic nerves and optic chiasm were difficult to evaluate because of striking contrast and artifacts from surrounding fat and CSF, respectively.

Cerebral Cortex and Subcortical White Matter

In the remainder of the cerebrum, the only consistent findings were of faint T1 shortening and very faint T2 shortening along the corticospinal tracts (Figs 1E–F and 2J). The anterior commissure and habenular commissure (Fig 1D) occasionally showed T1 shortening.

Discussion

The findings of this study establish that certain structures are consistently seen on MR imaging studies of the neonatal brain. A knowledge of these structures and their locations is critical for the proper interpretation of neonatal MR scans, particularly in those children with evidence of cranial neuropathies. Moreover, this study shows that many of the structures are seen better on T1-weighted images, whereas others are better seen on T2-weighted images. Finally, this study shows that the signal intensity of the gray matter structures within the neonatal brain is variable on both T1- and T2-weighted images.

The results of this study reveal that a large number of rather small structures, including many small cranial nerves and thalamic nuclei, can be identified regularly on MR studies of the neonatal brain. The ability to detect these nuclei, which were not consistently detected only 6 years ago (8), is probably the result of improvement in MR imaging hardware and software. However, it is important to note that most of these structures were not seen on every study. The most likely reason for missing these nuclei on some

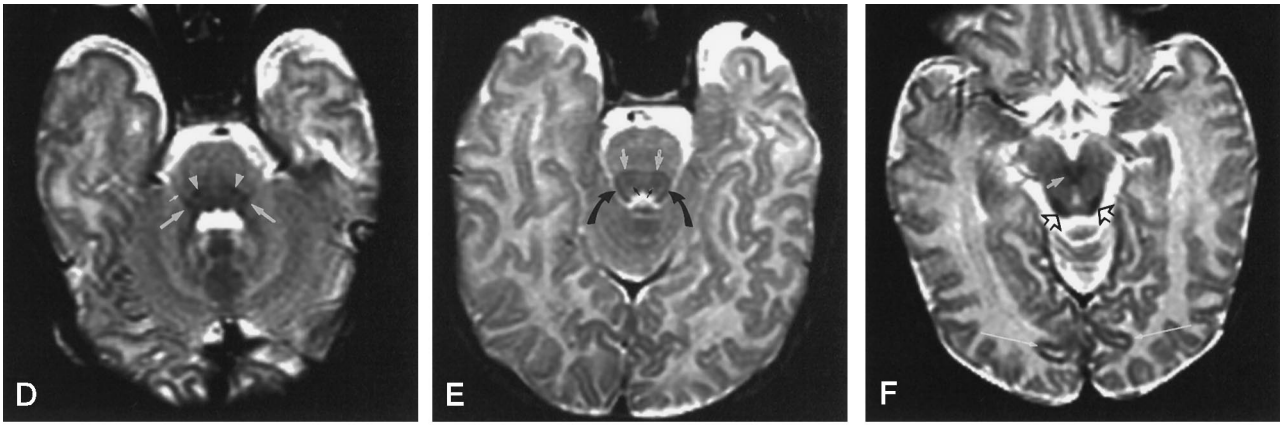

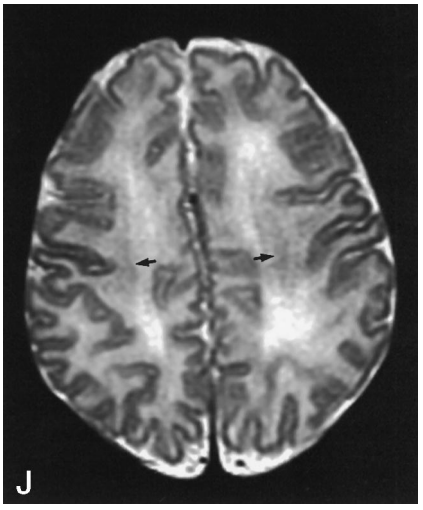

FIG 2. Axial spin-echo (3000/120/1) images.

A, Image at the level of the lower medulla shows low signal intensity (*arrows*) at the level of the nuclei cuneatus and gracilis.

B, Image in the upper medulla shows low signal intensity in the vestibular nuclei (*large straight arrows*), inferior cerebellar peduncles (*small straight arrows*), inferior olivary nuclei (*arrowheads*), and inferior cerebellar vermis (*curved arrows*).

C, Image at a similar level to *B*, but in a different patient, better shows the low signal intensity of the dentate nuclei (*white arrows*) and the flocculi (*black arrows*). Low signal intensity is also noted in the cerebellar vermis, vestibular nuclei, and inferior olivary nuclei, as in *B*.

D, Image at the level of the middle of the pons shows the main nuclei of the sixth (*black arrows*), seventh (*arrowheads*) cranial nerves and the spinal nucleus of the fifth (*large arrows*) cranial nerves. The intrapontine fascicle of the fifth nerve is seen coursing through the pons (*small arrow*).

E, Image at the level of the upper pons shows the medial lemnisci (*white arrows*), lateral lemnisci (*curved black arrows*), and the fibers of the superior cerebellar peduncles (*small black arrows*) as they course toward their decussation in the midbrain. It was unusual to see the structures this discretely.

F, Image at the level of the midbrain shows low signal in the region of the third nerve nuclei/interpeduncular nuclei (*short white arrow*) and at the nucleus of the inferior colliculus (*black arrows*). Not also the low signal intensity of the visual cortex (*long white arrows*) compared with most of the cortical gray matter.

G, Image at the level of the midbrain (different patient) shows the medial and lateral geniculate bodies (*large arrows*) and the oculomotor nuclei (*small arrows*) as regions of hypointensity.

H, Image at the level of the superior midbrain and inferior basal ganglia shows hypointensity of the subthalamic nuclei (*open arrows*) and the geniculate bodies, seen better on the left (*solid arrows*) than on the right.

I, Image at the level of the basal ganglia shows a curvilinear stripe of hypointensity in the lateral aspect of the putamina (*large solid white arrows*), a spot of hypointensity in the posterior limbs of the internal capsules (*small white arrows*), and a large focus of hypointensity in the ventrolateral thalami (*open arrows*). The left claustrum (*black arrows*) can be seen between the external and extreme capsules.

J, Image at the level of the centrum semiovale shows faint hypointensity in the midportion of the centrum (*arrows*) along the corticospinal tracts.

studies is the very small size of the structures and because a 1- or 2-mm gap was present between the imaging sections on our studies. It seems likely that a dedicated study of the brain stem, by obtaining contiguous or overlapping 3- or 4-mm sections (perhaps acquired in two consecutive sequences with an offset of 2 to 3 mm), should allow most of these structures, such as the pontine nuclei and the geniculate bodies, to be viewed very consistently. Alternatively, a high-resolution 3D acquisition technique (eg, spoiled gradient-recalled imaging, 3D fast low-angle shot, magnetization-prepared rapid acquisition gradient-echo) with a small (1- to 3-mm) partition size could be used. Identification of these structures may prove useful in the assessment of neonates with cranial neuropathies or other neurologic impairments. The higher resolution of our modern equipment also allowed us to separate the high T1-weighted signal of the posterior limb of the internal capsule from that of the adjacent globus pallidus on images at the level of the basal ganglia. Our images showed that only a small focus of T1-weighted shortening is present in the posterior limb of the internal capsule of the neonate at the level of the globus pallidus and that most of the hyperintensity is present in the globus pallidus (Fig 1D). In previous investigations, in which the signal of the capsule could not be distinguished from that of the pallidum, most of the high signal has been attributed to the internal capsule (1, 9).

The study also suggests that T1-weighted images show myelinated white matter tracts, which appear as regions of relative hyperintensity compared with unmyelinated white matter, better than gray matter structures. Gray matter structures are less hyperintense (have longer T1-weighted relaxation times) and are seen less well and less frequently. On T2-weighted images, however, the difference in signal intensity between gray matter and unmyelinated white matter

is much greater than on T1-weighted images; thus, gray matter structures, particularly brain stem and thalamic nuclei, are very conspicuous as foci of low signal intensity (Fig 2A–D). The reason that some of these gray matter structures, or some regions of gray matter structures, are better seen than others may relate to myelination as well. It is commonly known that axons run through gray matter structures and that some of these axons undergo early myelination (18, 19). Indeed, the nuclei that are best seen on these T2-weighted MR studies (Table 1) correspond almost exactly with those that have been shown to be myelinated at birth by Rorke and Riggs (19) and by Yakovlev and Lecours (18). Thus, it appears that myelinated nuclei are, in general, seen better than unmyelinated nuclei on T2-weighted images.

We were able to distinguish at least four levels of hypointensity on the MR images of the neonates in this study: unmyelinated white matter, unmyelinated gray matter, myelinated white matter, and myelinated gray matter. On the T1-weighted spin-echo images of neonates, unmyelinated white matter was most hypointense, followed, in order of increasing intensity, by unmyelinated gray matter, myelinated gray matter, and myelinated white matter. On T2-weighted spin-echo images of neonates, the unmyelinated white matter was the most hypointense, followed by the unmyelinated gray matter, myelinated white matter, and myelinated gray matter. Several possible explanations exist for the difference in signal intensity between the T1- and T2-weighted images. First, as Korogi et al (20) have discussed, it is likely that the changes in signal intensity of developing gray matter reflect the development of neurons, synapses, and oligodendrocytes, in addition to the changes in myelination. They postulate that maturational changes of neurons and, in particular, increasing synaptic density may reduce the amount of free water in the brain, resulting in shortening of the T2-weighted relaxation time. This theory is very reasonable and is consistent with the finding that many developmental changes, including chemical changes (21), increased local blood flow (3), increased glucose uptake (22), increased synaptic density (20), and increased myelination (19, 23), occur nearly simultaneously in specific regions of the developing brain. This explanation may help to explain why the intensities of mature gray matter differ on the different imaging sequences. An observation that seems confounding is that the myelinated medial globus pallidus is hyperintense on T1-weighted images but is not hypointense on T2-weighted images, whereas the similarly myelinated ventrolateral thalamic nuclei are minimally hyperintense on T1-weighted images but very hypointense on T2-weighted images (Figs 1D and 2I). It is clear that we still have a lot to understand regarding the processes that cause the T1 and T2 shortening in the developing brain.

It is reasonable to ask why we chose to study standard T1- and T2-weighted images at a time when fluid-attenuated inversion recovery (FLAIR) is the "hot" sequence. The answer is quite simple. In our experience, FLAIR is not a useful sequence in the neonate because it does not adequately show abnormalities and does not show good anatomic detail. Therefore, standard imaging sequences such as T1- and T2-weighted spin-echo sequences remain the mainstay of neonatal neuroimaging. We need to better understand the normal appearance of the brain on these sequences to be better diagnosticians for the neonate.

Conclusion

A large number of normal structures can be identified in the brain stem, cerebellum, and deep regions of the cerebrum on T1- and T2-weighted spin-echo studies of the neonatal brain. A knowledge of these structures is essential for proper interpretation of imaging studies of these patients.

References

1. Barkovich AJ, Kjos BO, Jackson DE Jr, **Norman D. Normal maturation of the neonatal and infant brain: MR imaging at 1.5 T.** *Radiology* 1988;166:173–180
2. Barkovich AJ. **Brain development: normal and abnormal. In: Atlas SW, ed.** *Magnetic Resonance Imaging of the Brain and Spine*. New York: Raven; 1991:129–175
3. Barkovich AJ, Hallam D. **Neuroimaging in perinatal hypoxic-ischemic injury.** *Ment Retard Dev Disabil Res Rev* 1997;3:28–414
4. Dietrich RB, Bradley WG, Zagaroza EJ, et al. **MR evaluation of early myelination patterns in normal and developmentally delayed infants.** *AJNR Am J Neuroradiol* 1988;9:69–76
5. Keeney SE, Adcock EW, McArdle CB. **Prospective observations of 100 high-risk neonates by high field (1.5 Tesla) magnetic resonance imaging of the central nervous system, I: intraventricular and extracerebral lesions.** *Pediatrics* 1991;87:421–430
6. Keeney SE, Adcock EW, McArdle CB. **Prospective observations of 100 high-risk neonates by high field (1.5 Tesla) magnetic resonance imaging of the central nervous system, II: lesions associated with hypoxic-ischemic encephalopathy.** *Pediatrics* 1991;87:431–438
7. Martin E, Boesch C, Zuerrer M, et al. **MR imaging of brain maturation in normal and developmentally handicapped children.** *J Comput Assist Tomogr* 1990;14(5):685–692
8. Martin E, Krassnitzer S, Kaelin P, Boesch C. **MR imaging of the brainstem: normal postnatal development.** *Neuroradiology* 1991;33:391–3959
9. McArdle CB, Richardson CJ, Nicholas DA, Mirfakhraee M, Hayden CK, Amparo EG. **Developmental features of the neonatal brain: MR imaging, Part I: gray-white matter differentiation and myelination.** *Radiology* 1987;162:223–229
10. Sie LTL, van der Knaap MS, van Wezel-Meijler G, Valk J. **MRI assessment of myelination of motor and sensory pathways in the brain of preterm and term-born infants.** *Neuropediatrics* 1997;28:97–105
11. Staudt M, Schropp C, Staudt F, et al. **MRI assessment of myelination: an age standardization.** *Pediatr Radiol* 1994;24:122–127
12. Steinlin M, Dirr R, Martin E, et al. **MRI following severe perinatal asphyxia: preliminary experience.** *Pediatr Neurol* 1991;7:164–170
13. Staudt M, Schropp C, Staudt F, Obletter N, Bise K, Breit A. **Myelination of the brain in MRI: a staging system.** *Pediatr Radiol* 1993;23:169–176
14. van de Bor M, Guit GL, Schreuder AM, Wondergem J, Vielvoye GJ. **Early detection of delayed myelination in preterm infants.** *Pediatrics* 1989;84:407–411
15. van der Knaap MS, Valk J. **MR imaging of the various stages of normal myelination during the first year of life.** *Neuroradiology* 1990;31:459–470
16. van der Knaap MS, van Wezel-Meijler G, Barth PG, Barkhof F,

Adèr HJ, Valk J. **Normal gyration and sulcation in preterm and term neonates: appearance on MR images.** *Radiology* 1996;200: 389–396
17. Bayley N. *The Bayley Scales of Infant Development II*. New York: New York Psychological Corp; 1993
18. Yakovlev PI, Lecours AR. **The myelogenetic cycles of regional maturation of the brain.** In: Minkowski A, ed. *Regional Development of the Brain in Early Life*. Oxford: Blackwell; 1967:3–70
19. Rorke LB, Riggs HE. *Myelination of the Brain in the Newborn*. Philadelphia: Lippincott; 1969:28
20. Korogi Y, Takahashi M, Sumi M, et al. **MR signal intensity of the perirolandic cortex in the neonate and infant.** *Neuroradiology* 1996; 38:578–584
21. Penrice J, Cady EB, Lorek A, et al. **Proton magnetic resonance spectroscopy of the brain in normal preterm and term infants and early changes after perinatal hypoxia-ischemia.** *Pediatr Res* 1996; 40:6–14
22. Chugani HT, Phelps ME, Mazziotta JC. **Positron emission tomography study of human brain functional development.** *Ann Neurol* 1987;22:487–497
23. Azzarelli B, Meade P, Muller J. **Hypoxic lesions in areas of primary myelination.** *Childs Brain* 1980;7:132–145